Laboratori Nazionali di Frascati

LNF-90/016(R)
21 Marzo 1990

L. Serafini, M. Ferrario, C. Pagani, A. Ghigo, P. Michelato and A. Peretti:

X-VUV POSSIBLE FEL EXPERIMENTS WITH THE ARES SC LINAC

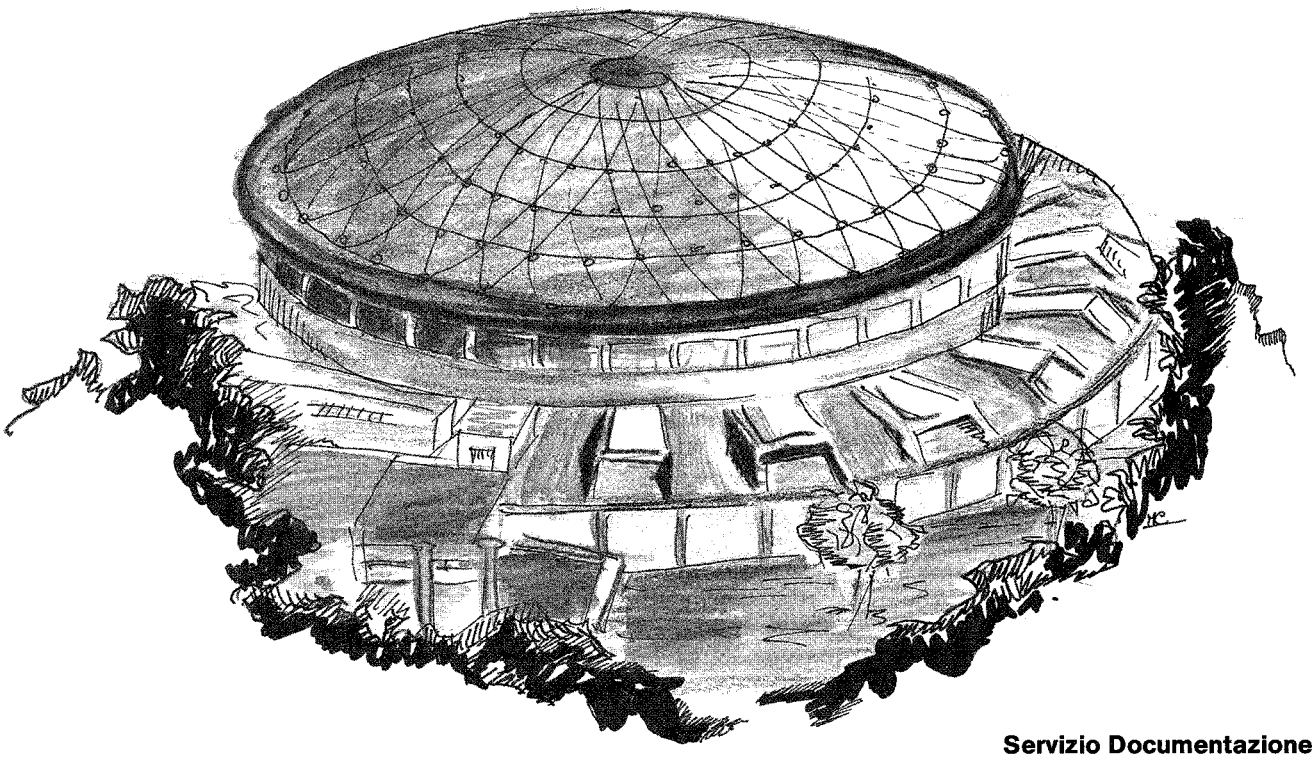

Servizio Documentazione
dei Laboratori Nazionali di Frascati
P.O. Box, 13 - 00044 Frascati (Italy)

INFN - Laboratori Nazionali di Frascati
Servizio Documentazione

LNF-90/016(R)
21 Marzo 1990

X-VUV POSSIBLE FEL EXPERIMENTS WITH THE ARES SC LINAC

L.Serafini*, M.Ferrario*, C.Pagani*, A.Ghigo, P.Michelato*, A.Peretti*

INFN Laboratori Nazionali di Frascati - P.O. BOX 13 - 00044 Frascati
* INFN and Università di Milano - Via Celoria 16 - 20133 Milano

1 - Introduction

The availability of intense electron beams of high quality makes the ARES SC LINAC complex a unique facility to perform several experiments in the X-ray VUV FEL mainstream. In this paper we present a feasibility study of a device able to generate coherent radiation of high brightness in the soft X-ray VUV spectral region (photon energies in the 10-120 eV range), together with a tentative list of the possible FEL experiments.

Detailed, but still preliminary, numerical simulations will be extensively reported: they anticipate the FEL performances and support the enclosed lists of parameters concerning the beam quality requirements and the wiggler characteristics. These simulations have been carried out taking into account a new recently proposed technique: the "ion focussing" of the beam, achieved with a pre-ionized plasma channel added inside the beam pipe in the wiggler[5].

Some new applications of old ideas are also presented here for the first time, in the last two sections: they deal with the subject of coherent spontaneous emission. Inside our range of radiation wavelengths such new schemes will open the possibility to obtain coherent radiation wavelength of ≈ 50 Å, in the so called "water window". The new experimental physics field which may be explored with such a radiation source is, in our opinion, as wide as needed to justify the big effort to build such a device.

Indeed, it is well known that the shorter is the radiation wavelength, the higher must be the beam quality needed to operate a single pass high-gain FEL in the SASE (Self Amplified from Spontaneous Emission) mode. As shown elsewhere[1], the choice of a low frequency and a superconducting structure for the beam acceleration plays a crucial role in minimizing the beam quality degradation through the LINAC. In this respect, the injection system turns out to be one of the most important part of the whole complex.

It is worthwhile to mention that the SC LINAC will also constitute an experimental tool to study the beam-beam and the beam-radiation field interactions: such effects are of great relevance in the design of all future e^+ e^- TeV colliders. A better understanding of the beamstrahlung processes will surely allow to improve the feasibility and the performances of such machines.

2 - One Dimensional Model Predictions.

As elsewhere presented in more detail[1], the expected beam characteristics at the LINAC output, for FEL experiments, can be summarized as shown in Table 1. Having available beams with a relativistic factor, γ, in the range 600÷1200, one can easily observe that the resonant radiation wavelength, given by the usual FEL resonance relationship, lies in the range 200-20 nm (for the first harmonic) when wigglers with typical periods of a few centimetres are considered. In fact the FEL resonance equation is:

$$\lambda_r = \frac{\lambda_w (1 + a_w^2)}{2\gamma^2 n}$$

where: λ_w is the wiggler period, λ_r the n-th harmonic radiation wavelength and a_w is the dimensionless vector potential of the wiggler. In a planar wiggler a_w is related to the peak magnetic field, B_w, by the formula: $a_w \approx .66\, \lambda_w$ [cm] B_w [T].

Unfortunately, the scaling law for the exponential growth of the radiation field is quite unfavourable in the very short wavelength domain. The gain length, L_g, i.e. the length over which the radiation field intensity grows by a factor e, scales indeed like the beam energy divided by the cubic root of the wiggler period, as in the following formula, which holds in the cold-beam limit and before saturation[2]:

$$L_g \approx \frac{\gamma}{\sqrt[3]{J \lambda_w B_w^2}}$$

where J is the beam current density.

Table 1 - Expected Beam Characteristics

Beam energy	[MeV]	300 ÷ 580 (820*)	
Peak current	[A]	400	1000
Norm. transv. emitt.	[m rad]	$4 \div 8 \cdot 10^{-6}$	$4 \div 5 \cdot 10^{-5}$
Relative energy spread		$.5 \div 1 \cdot 10^{-3}$	$2 \div 5 \cdot 10^{-3}$

* Eventually obtainable with a second recirculation.

To reach the VUV to soft X-ray domain (radiation wavelength between 10 and 100 nm) high γ and short wiggler periods are both needed, B_w being dependent on λ_w as will be shown later. That implies that fine and intense beams must be used in order to overcome by the increase in current density the corresponding increase of the gain length.

It is well known that in an untapered wiggler, because of the exponential growth of the radiation field, once the high gain regime is achieved, intensity reaches saturation after a typical length of the order of $4 \pi L_g$: at that point the radiation power, P_r, is roughly given by the beam power, P_b, times the Pearce parameter, ρ, ($\rho = \lambda_w/4\pi L_g$), that is $P_r = \rho P_b$[2]. Then, the saturated radiation power comes out invariant with respect to the beam energy.

A more important scaling law sets a threshold for the radiated power, which must be high enough to ensure that the quantum fluctuations in the photon beam do not destroy the coherence properties of the radiated field: the condition is given by

$$P_r\,[\mathrm{MW}] > \frac{5.9\ 10^{-6}}{\lambda_r^{\,2}\, q_f^{\,2}}$$

where q_f is the maximum quantum fluctuation compatible with the radiated field coherence; q_f should actually be of the same order of magnitude as the ratio between the incoherent radiated power and the coherent one, so as to ensure that the incoherent quantum noise does not significantly perturb the coherence of the radiated field. The previous relationship comes from the scaling of the quantum fluctuation with the inverse square root of the number of photons per wavelength[3].

The requirement of a radiated power scaling like the square of the frequency (i.e. the square of the photon energy) actually sets one of the major limits in going towards the X-ray domain.

The transverse size, r_b, of the electron beam in a wiggler with appropriate shaping of the pole face is given by[4]:

$$r_b = \sqrt{\frac{\varepsilon_n \lambda_\beta}{2\pi\gamma}} \qquad \text{being:} \qquad \lambda_\beta = \frac{\sqrt{2}\,\gamma\lambda_w}{a_w} H \tag{1}$$

Where ε_n is the transverse normalized emittance of the beam and the parameter H represents the effect of the ion focussing in decreasing the betatron wavelength λ_β. In absence of ion focussing H = 1; the ion focussing effect makes H < 1 [5].

The relevance of producing low emittance beams and to increase the focussing strength of the wiggler optics is then straightforward. The ion focussing scheme consists essentially in producing, inside the beam pipe along the wiggler, a tenuous ion channel: this is generated by injecting an intense leading low energy (≈ 300 MeV) electron beam into a low pressure helium column. The beam ionizes the helium gas and the space charge field of the beam ejects the detached plasma electrons from the beam vicinity. The charge of the second injected electron beam is partially, or totally (depending on the helium pressure) compensated in passing through the ion channel. The pinch field acting on the beam increases the focussing strength, decreases the beam transverse size and produces a substantial gain length contraction. Finally, it is worthwhile noting that the gain length scales with the cubic root of H.

Two major constraints on the quality of the electron beam injected into the wiggler must be taken into account when the cold beam limit approximation is abandoned. The transverse and the longitudinal phase spaces of the electron and of the photon beams must be matched if the interaction between the two beams has to be ensured all along the wiggler, in order to set up the energy exchange which is the basic condition to achieve an exponential gain in the radiated field power. For the transverse phase space one must match the emittance of the electron beam with the emittance of a diffraction limited radiation beam; this means that[6]:

$$\varepsilon_n = \frac{\lambda_r \gamma}{2\pi} f_1 \tag{2}$$

where f_1 must be kept below 1 (as discussed later).

Since the line-width of the radiated field at saturation is of the order of ρ, the energy spread of the injected beam must be less than this quantity: in practice it has been found from simulations[7] that the proper condition is given by:

$$\frac{\Delta\gamma}{\gamma} < \frac{\rho}{4}$$

A last condition comes from the requirement that diffraction does not remove radiation from the edge of the electron beam over a length shorter than the gain length; this requires the Rayleigh length, Z_r, to be larger than the gain length, L_g[8]:

$$L_g = Z_r f_3 \qquad \text{being} \quad f_3 \leq 1 \qquad \text{and} \qquad Z_r = \frac{\pi r_b^2}{\lambda_r}$$

In some sense this condition sets a limit to the extent to which the ion focussing can be pushed: a reduction of the beam radius causes a decrease of the gain length, scaling like the square of the cubic root of the radius, but unfortunately also the Rayleigh length decreases scaling like the square of the radius. The best compromise on the effectiveness of the ion focussing technique is reached when $f_3 \approx 1$, that is when the diffracted power is not higher then the power increase due to the exponential gain. A further ion focussing increase, making $f_3 > 1$, no longer improves the FEL performance, as will be shown later.

Taking into account what could be a typical step-by-step upgrading of the SC LINAC facility, especially in terms of beam current and output emittance, we listed in Table 2 the corresponding envisageable FEL experiments: the table has been divided into four sections, to list the quantities related to the beam requirements, to the wiggler characteristics, to the FEL radiated power and to the above mentioned parameter f_i, that control the validity of the one-dimensional evaluation. The quantity $f_2 \equiv f_1^2 \cdot f_3$ must be less than 1[5]. The two parameters S and K measure the slippage effect and the superradiance behaviour of the FEL, as defined in ref.(9).

Moving from left to right on Table 2 the difficulty of the FEL experiment grows, both because of the tighter beam quality requirements and of the difficulties in manufacturing the required wiggler.

A few comments on the beam parameters are in order:

- the first anticipated beam will be produced by the LINAC without any recirculation, with a peak current of 200 A and a transverse normalized emittance (rms value of $1 \cdot 10^{-5}$) fully consistent with the preliminary design of the injection system[1].
- the energy spread shown in the Table takes into accounts the effect of the longitudinal wake-field excited inside the RF cavities: here it must be remarked that such low values for the energy spread are made possible only by the low RF frequency selected for the LINAC.

Table 2 - Possible FEL Experiments

Beam energy, T	[MeV]	292	500	580	580	B
Peak current, I_{peak}	[A]	200	400	400	400	E
Bunch length, σ_b	[mm]	.3	.3	.2	.2	A
Norm emittance, ε_n	[m rad]	$1{\cdot}10^{-5}$	$8{\cdot}10^{-6}$	$1.5{\cdot}10^{-6}$	$4{\cdot}10^{-6}$	M
Energy spread, rms	[keV]	±100	±150	±200	±200	
Wiggler period, λ_w	[cm]	3	3	2	2	W
Peak mag. field, B_w	[T]	.75	.75	1.	1.	I
Wiggler parameter, a_w		1.49	1.49	1.32	1.32	G
Wiggler pole gap	[cm]	.9	.9	.45	.45	G
Max. field for SmCo	[T]	.8	.8	1.1	1.1	L
Ion focussing param, H		1	1	1	.38	E
Beam radius, R_b	[μm]	210	190	67	67	R
Rad. Wavelength, λ_r	[nm]	133	50	21	21	
Pierce parameter, ρ		$2.1{\cdot}10^{-3}$	$1.7{\cdot}10^{-3}$	$2.0{\cdot}10^{-3}$	$2.0{\cdot}10^{-3}$	F
Photon energy	[eV]	9	25	58	58	E
Saturation power, P_{sat}	[MW]	190	380(40*)	550(320*)	550	L
Gain length, L_g	[m]	.66	.81(1.36*)	.46(.62*)	8.2	
Intensity at saturation	[W/cm^2]	$4.2\cdot10^{10}$	$1.0\cdot10^{11}$	$1.2\cdot10^{12}$	$1.2\cdot10^{12}$	
$(\Delta\gamma/\gamma)/(\rho/4)$		1.06	1.4	1.15	1.15	
Quantum fluctuation param., q_f		$4{\cdot}10^{-6}$	$8{\cdot}10^{-6}$	$1.6{\cdot}10^{-5}$	$1.6{\cdot}10^{-5}$	C
$f_1 \equiv 2\,\pi\,\varepsilon_n/(\lambda_r\,\gamma)$		.79	1.02	.34	1.04	H
$f_2 \equiv f_1^2\, f_3$		.59	.65	.11	.97	E
$f_3 \equiv L_g/Z_r$		.95	.62	.99	.9	C
S		.15	.056	.053	.053	K
K		.007	.003	.002	.002	

* FRED-3D calculations.

Therefore the first FEL experiment will be just a standard single pass FEL amplifier at a resonance radiation wavelength of ≈ 133 nm, where an input signal is available by a Nd-YLF laser multiplied in frequency at the eighth harmonic by a passage through a triple BBO crystal[10]. A few MW of peak power can be delivered in 50 ps pulses at a repetition rate of 1 kHz. The wiggler parameters are consistent with the Halbach scaling law for hybrid magnet wigglers[11]: with a gap of 9 mm the maximum allowed peak field is .8 T, versus the selected .75 T.

Integrating numerically the standard Compton-FEL equations for the one-dimensional model, we observe a saturated power of 190 MW after 8 meters of wiggler, when a 1 MW of input power has been injected into the wiggler: the value of ρ is in this case $\approx 2 \cdot 10^{-3}$. As shown in Table 2, the test quantities are all under control, especially the f_1 parameter, while the slippage and the superradiance parameters, being very small, indicate that the steady state regime is adequate to describe the exponential growth of the FEL radiation field.

The other three columns of Table 2 show the parameters required to operate a FEL amplifier starting from spontaneous emission, at radiation wavelengths of 50 and 21 nm, respectively. The beam must be recirculated once in the second stage of the LINAC to raise the energy to roughly .5 GeV ; the peak current increases up to 400 A, as anticipated[1]. The input signal is in this case the incoherent spontaneous synchrotron emission, P_{inc}, which reaches a few tens of kW per meter of wiggler, as estimated by the formula[12]

$$P_{inc}[\mathrm{kW/m}] = 1.9 \frac{a_w^2 (1 + a_w^2)\, I[\mathrm{A}]}{\lambda_w[\mathrm{cm}]\ \lambda_r[\mathrm{nm}]}$$

The fourth column deals with a particular application of the ion focussing technique: since the required emittance, as shown in the third column, is too small, a slight amount of ion focussing (H = .38) allows to increase the maximum emittance by a factor of three, keeping ρ constant. Further comments on this case will be given in the next section, where the 3-D simulation results are presented.

3 - Numerical Simulations of the High Gain FEL

The computer code FRED-3D has been used[20] to simulate the behaviour of the coupling between the electron beam and the radiation field induced by the wiggler field, for a 3-D beams (i.e. taking into account the transverse phase space evolution for both the particles and the field). Slippage effects are in this frequency-domain and, for millimetre long electron bunches, quite negligible; the steady state approximation used by FRED-3D is then completely adequate.

The input electron beam is actually mono-energetic, but it is well known that for energy spreads below the value given by the Pellegrini's rule[6] no serious deterioration of the FEL performance is to be expected. The field power growth is shown on a logarithmic scale, in Fig. 1, for the case of the parameters presented in column 2 of Table 1, i.e. for a radiation wavelength of 50 nm.

After three meters of lethargy, the signal grows exponentially up to 30 MW; the latter value is reached at the end of a 20 m long wiggler. Since the gain is about 3.2 dB/m, as shown in

Fig. 2, a further 3.5 meters of wiggler length would be needed to reach the 1-D estimated saturation power at 380 MW.

The observed gain length, L_g, is therefore 1.36 m, which must be compared to the value of .81 m, predicted by the 1-D model. The discrepancy can be understood taking into account that the Rayleigh length, Z_r, for this case is slightly above the gain length. Since the 1-D model is valid in the limit $Z_r >> L_g$ (i.e. $f_3 << 1$), the gain decrease due to diffraction effects cannot be accounted for by the 1-D model. The same holds for the transverse phase space effects: since the emittance is just above threshold, ($f_1 = 1.02$), one must expect the 1-D calculation to predict a higher gain than the 3-D one.

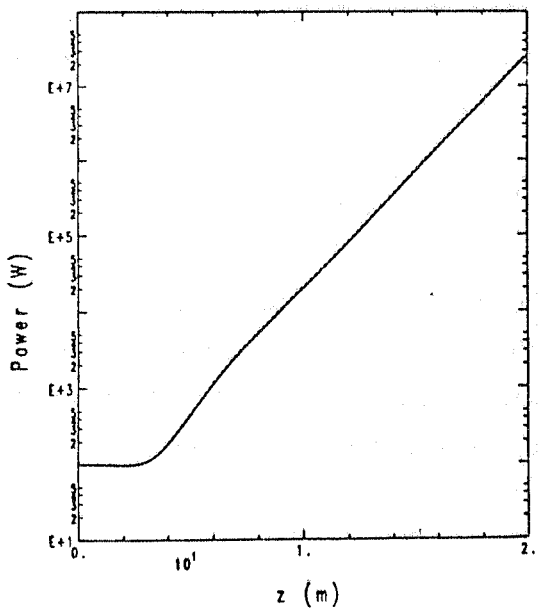

Fig. 1 - Field power growth, on a log scale, with the parameters presented in column 2 of Table 1.

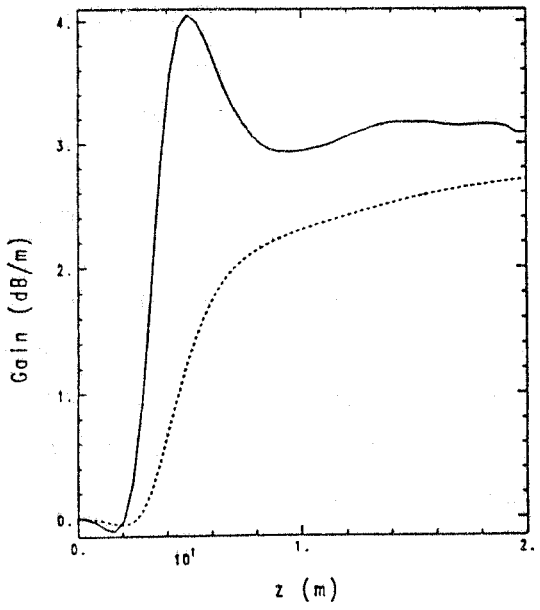

Fig. 2 - Incremental (solid line) and average (dashed line) gain along the wiggler for the case of Fig. 1.

We want to point out that a coherent input signal of 100 W has been used to start the FEL, even though no coherent signal is available at this wavelength (50 nm). In particular, since FRED-3D is not able to simulate the start up from the Schottky noise or from the incoherent spontaneous emission, 100 W has to be taken just as a reference value, to be compared to the incoherent synchrotron radiation power, which is in this case 36 kW/m. Harmonic switching (see below) or other exotic ideas like the SHOK scheme[13] could overcome the input signal problem.

The full exploitation of the ion focussing technique has been carefully studied for the case of the 21 nm radiation wavelength, with a 580 MeV beam at 400 A (third column of Table 2). The field power computed by FRED-3D along the wiggler is shown in Fig. 3 and 4 on logarithmic and linear scales, respectively. The input signal is still a 100 W coherent field. The incoherent

synchrotron radiation power is in this case 85 kW per meter of wiggler, or, equivalently, 1.7 kW per wiggler period.

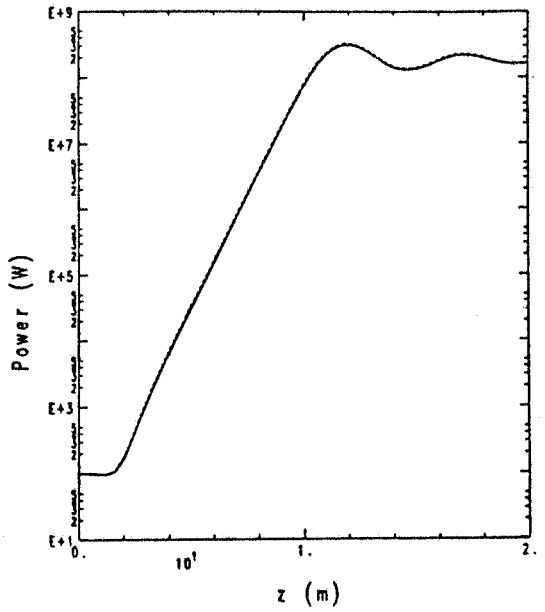

Fig. 3 - Field power growth, on a log scale, with the parameters presented in column 3 of Table 2.

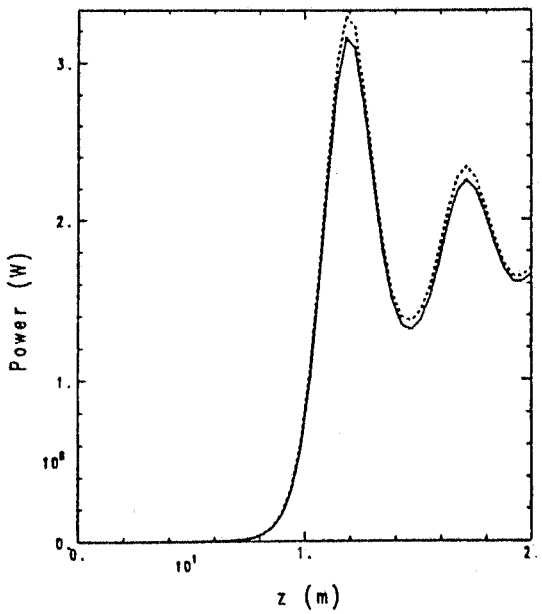

Fig. 4 - Same as Fig. 3, but on a linear scale. The power is in units of 10^8 W.

After 2 meters of lethargy the exponential gain sets in and the radiation field reaches the 320 MW saturation power level at z = 12 m: the corresponding intensity is $1.2 \cdot 10^{12}$ W/cm^2, confined in a narrow cone of about .1 mm rms radius and $1.1 \cdot 10^{-5}$ rad rms angular width. In Figs. 5 and 6 the intensity profiles are plotted as functions of the transverse coordinate x of the wiggler, at the entrance (z = 0) and at the exit of the wiggler (z = 20 m) respectively.

The input field is a gaussian laser beam focussed at z = 0. At the wiggler exit the intensity profile, due to diffraction effect, shows that some radiation escapes from the electron beam: the gaussian fit (dashed curve in Fig. 6) reveals that the optical guiding and the diffraction along the wiggler produce a distortion of the intensity profile, which is no longer gaussian. It should be noted that the peak value of Fig. 6 ($5 \cdot 10^{11}$) is lower than the peak value ($1.2 \cdot 10^{12}$) at saturation (z = 12 m).

Moreover, the phase profile of the radiation field at z = 20 m, shown in Fig. 7, indicates that the radiation beam is de-focussed, since the phase increases off-axis.

The "natural" betatron wavelength, λ_β, for this case is 24.5 m, which gives an rms beam radius in the wiggler of about 53 microns with a normalized rms emittance of 1.5 mm mrad. The incremental gain is shown (solid line) in Fig. 8: with an average value of 7 dB/m during the exponential growth, the gain length is approximately .62 m, slightly above the 1-D predicted one.

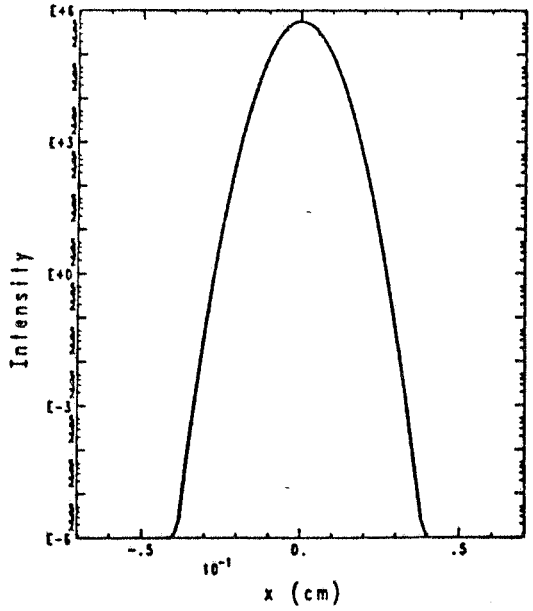

Fig. 5 - Intensity profile as a function of the transverse coordinate x of the wiggler at the start-up (z = 0 m), for the case of the parameters presented in column 3 of Table 2.

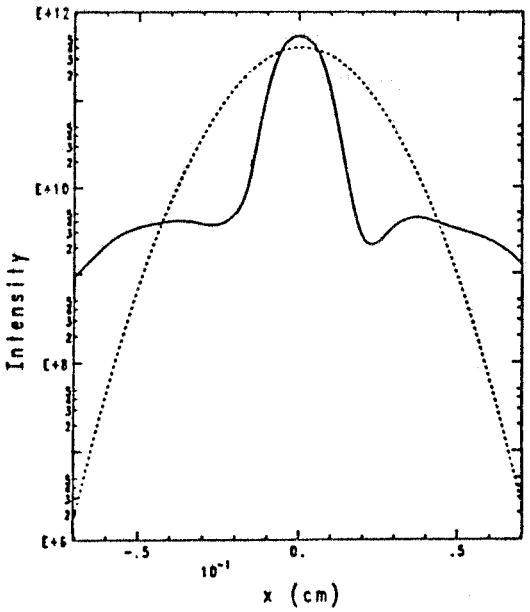

Fig. 6 - As Fig. 5 at the end of the wiggler (z = 20 m). Actual intensity (solid line) and gaussian fit (dashed line).

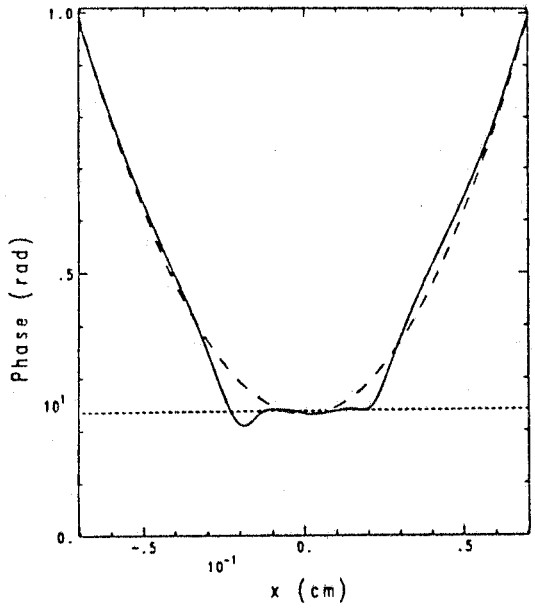

Fig. 7 - Radiation field phase profile (solid line) and its gaussian fit (dashed line) at z = 20 m.

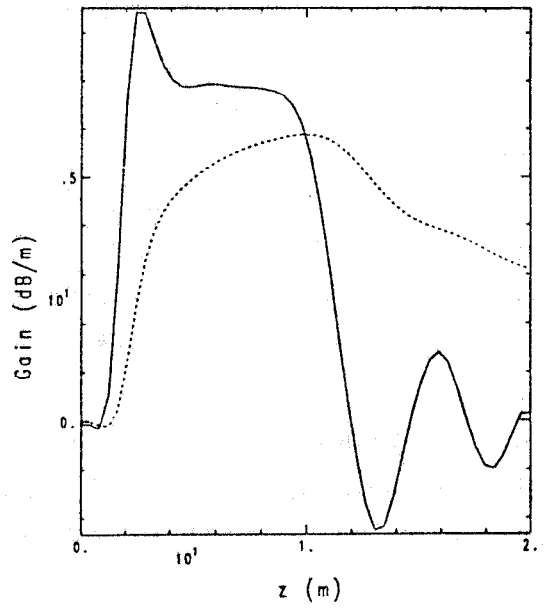

Fig. 8 - Incremental gain (solid line) and average gain (dashed line).

The total gain is about 65 dB after 12 metres of wiggler. Since the Rayleigh length is .41 m, the diffraction effects are probably responsible for such a decrease in the gain.

Introducing some amount of ion focussing one can decrease the betatron wavelength and squeeze the electron beam. In Fig. 9 is presented the radiated field power produced by reducing by a factor ten the betatron wavelength, i.e. by setting H = 0.1.

The saturation is reached at z = 8 m, with a wiggler much shorter than the previous one (H = 1, no ion focussing), but the saturation level is slightly lower: 250 MW versus 320 MW of the no-ion focussing case.

The peak field intensity at saturation, I_{sat}, is about $4.4 \cdot 10^{12}$ W/cm^2, with a spot radius of .6 mm and an rms angular divergence of $1 \cdot 10^{-5}$ rad. The incremental gain has now a plateau at 10 dB/m, with a total gain of 64 dB along the 8 meter wiggler.

The intensity profile is plotted in Fig. 10, at the wiggler exit. The exit profile exhibits very clearly the substantial fraction of field escaped from the electron beam, which has a maximum radius of about 50 microns.

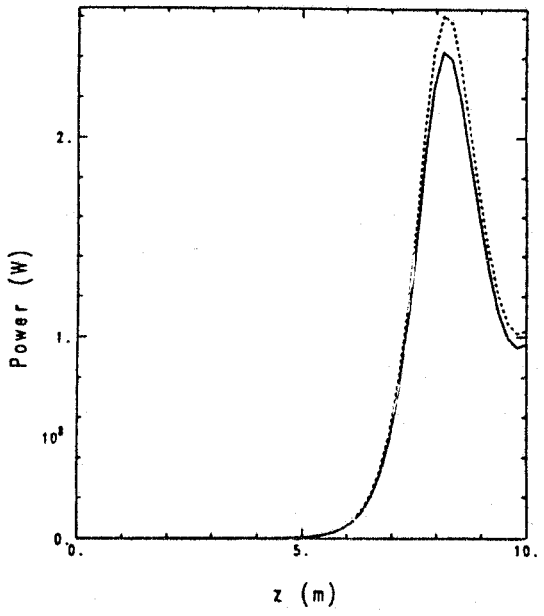

Fig. 9 - Radiated field power produced by reducing the betatron wavelength by a factor ten, i.e. setting H = 0.1.

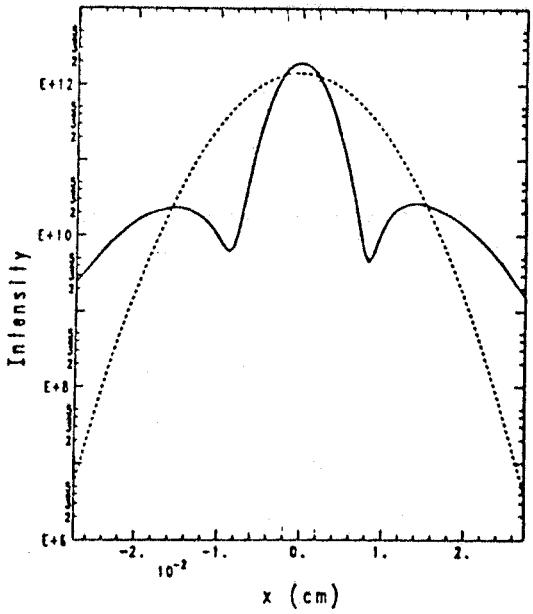

Fig. 10 - Intensity profile at the wiggler exit. The exit profile exhibits very clearly the substantial fraction of field escaped from the electron beam.

The optical guiding applied by the electron beam on the laser field is however better evidenced by the phase profile of the laser field, plotted in Fig. 11 at the wiggler exit: inside the electron beam, i.e. for x < 60 microns, the field phase decreases with the transverse coordinate, then the optical beam is converging. Outside the electron beam the field phase is instead strongly increasing, showing that the optical beam is defocussed in that region. The electron beam acts on the laser field as an optical fiber with a high refractive index. The optical guiding, already observed elsewhere [21], is stronger during the exponential gain than after saturation. That is clearly shown in Fig. 12, where the iso-intensity curves are plotted in the (x,z) plane for the case without the ion focussing: the laser beam is squeezed and focussed whenever the field is growing, i.e. the gain is positive.

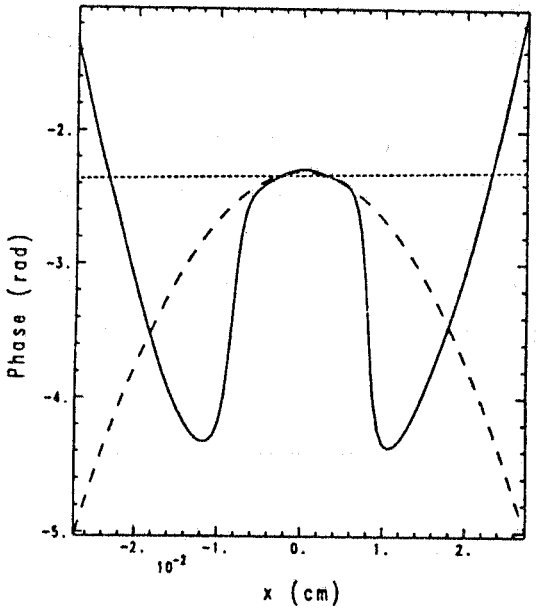

Fig. 11 - Phase profile of the laser field at the wiggler exit (solid line) and its gaussian fit (dashed line).

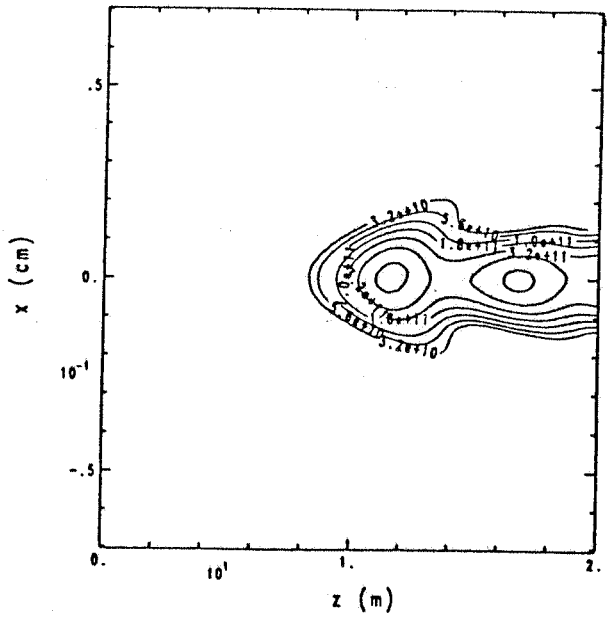

Fig. 12 -Iso-intensity curves, plotted in the (x,z) plane for the case without ion focussing.

The effect of ion focussing in decreasing the gain length has been explored performing FEL simulations with FRED-3D also at H = .75 and at H = .2. The results are summarized in Fig. 13, where the gain length observed in the FRED-3D calculations is plotted (dashed line) versus the betatron wavelength (H = 1 corresponds to λ_β = 24.5 m). The solid line in the same figure represents the gain length scaling as $H^{1/3}$, as predicted by the 1-D model: the gain length observed in the 3-D calculations then indicates that the FEL performance is enhanced by the ion focussing technique, but not as much as one would expect from the 1-D model considerations. That can be explained observing the dashed line plotted in Fig. 13, showing the f_3 coefficient, which gives the ratio between the gain length and the Rayleigh length: this ratio grows quickly above 1, indicating that diffraction effects become more and more relevant for the FEL performance.

It can be therefore concluded that the maximum benefit from the ion focussing technique can be obtained not by increasing the FEL performance, keeping constant the beam parameters, but relaxing the beam quality requirements keeping unaltered the gain length. It can be easily seen from equation (1) that the emittance can be scaled like the inverse of the amount H of ion focussing applied, keeping constant the beam radius, hence the gain length. One can therefore reduce the tight requirement on the beam emittance shown in the third column of Table 2 and list a new set of parameters in the fourth column, by simply scaling the emittance by a factor 2.7 and taking H = .38. In this way the gain length should stay constant since the Rayleigh length is

not changed (the beam radius is not varied) and the FEL performances are unaltered but achieved with a beam which is now consistent with the ones of Table 1. The f_1 parameter is still within the safety range $f_1 \approx 1$, the quantum fluctuations parameter being very low, $q_f = 1 \cdot 10^{-5}$.

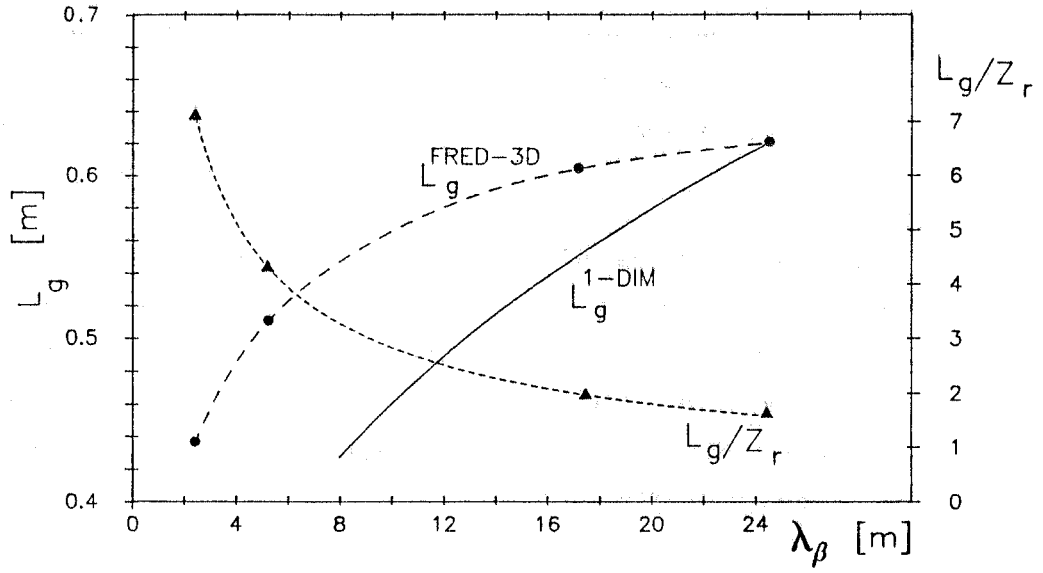

Fig. 13 - Effect of the ion focussing in decreasing the gain length (see text for details).

At 250 MW of peak power the number of photons per bunch is $3 \cdot 10^{13}$. With a bunch length of 1.2 ps the number of wavelengths contained in the laser pulse will be of the order of $2 \cdot 10^4$ with about $1 \cdot 10^5$ electrons per wavelength.

Since the maximum electron beam wiggle amplitude is in the range of 5 microns, very small with respect to the beam size, no serious problems are envisaged for the production of a uniform ion channel over the ± 100 microns of the beam transverse size.

4 - High Gain Optical Klystron and the Coherent VUV

The Self Amplified Spontaneous Emission (SASE) regime of an FEL allows to produce coherent VUV and soft-X-ray radiation starting from the incoherent spontaneous emission in the wiggler. In such a regime, the incoherent radiation, having an optical power proportional to the number of the electrons, is amplified by the electron beam in a single pass through the wiggler. The stimulated radiation grows exponentially to a saturation level which is proportional to $N^{4/3}$, N being the number of electrons in the bunch.

Beside the problems arising from the wiggler length needed to achieve saturation starting from the incoherent spontaneous emission (they will be discussed in the next section), one of

the major points is that the coherence of the output signal is lower than that obtainable from an FEL amplifier with a coherent input signal.

The coherence length of the output signal produced in the SASE regime is indeed given roughly by the slippage length: since the electrons interact with one another via the common radiation field, the interaction length is equal to the slippage length, hence the photons separated by more than the slippage length are of course decoupled. Therefore, the start up of the field amplification process from photon and electron populations which are both randomly distributed in phase cannot assure a narrow bandwidth and a coherent output signal.

Since the availability of coherent input signals (i.e. of a photon population peaked around a given phase) in the UV region decreases strongly with the wavelength, one could try to start with a "coherent" beam instead of a coherent input signal, i.e. with a bunched beam. The start up from a pre-bunched beam ensures a higher coherence of the radiation since the spontaneous emitted photon population is no longer randomly distributed in phase, but is peaked in phase around the electron beam bunching phase[14].

In Figs. 14 a and b the longitudinal phase-space for the electron beam of the FRED-3D simulation previously discussed is shown at two different positions along the wiggler:

- at z = 4 m, where the field power is still a few orders of magnitude lower than the saturation level, the beam has achieved an energy spread from the input signal but is still distributed fairly uniformly in phase. Since the wiggler field is dispersive, the energy spread will be transformed, along the wiggler, into a phase spread
- at z = 8 m, near saturation, the phase space appears like in Fig. 14 b, where the beam has achieved a substantial bunching, being well known that the bunching in the exponential regime grows exponentially too (the bunching parameter b is defined, as usual, $b=\langle e^{i\theta}\rangle$, where the average $\langle\rangle$ is performed over the θ electron phase distribution).

Integrating numerically the 1-D FEL equations[9] in the Compton limit ($\rho<<1$) one finds that, starting with a signal six orders of magnitude lower than the saturation level (in the present case 100 W), the field power saturates at 550 MW after 10.5 meters of wiggler length, and the bunching grows up to $\approx.7$ just before saturation, as shown in Fig. 15, according to the sets of parameters presented in Table 2, column 3.

Starting from these considerations and following the scheme of the optical klystron[15], we propose to separate the wiggler into two parts: the first one acts as a buncher and the second one as a radiator. If the two parts are decoupled, that is the radiation generated in the buncher is discarded, the radiator works as a generator of coherent spontaneous radiation at its proper resonant wavelength. In other words, truncating the exponential gain at a suitable point close to

saturation and discarding the radiated field generated so far (which is scarcely coherent), one can get a bunched beam able to radiate coherent synchrotron radiation, in a transient "superradiant" regime involving the overall beam.

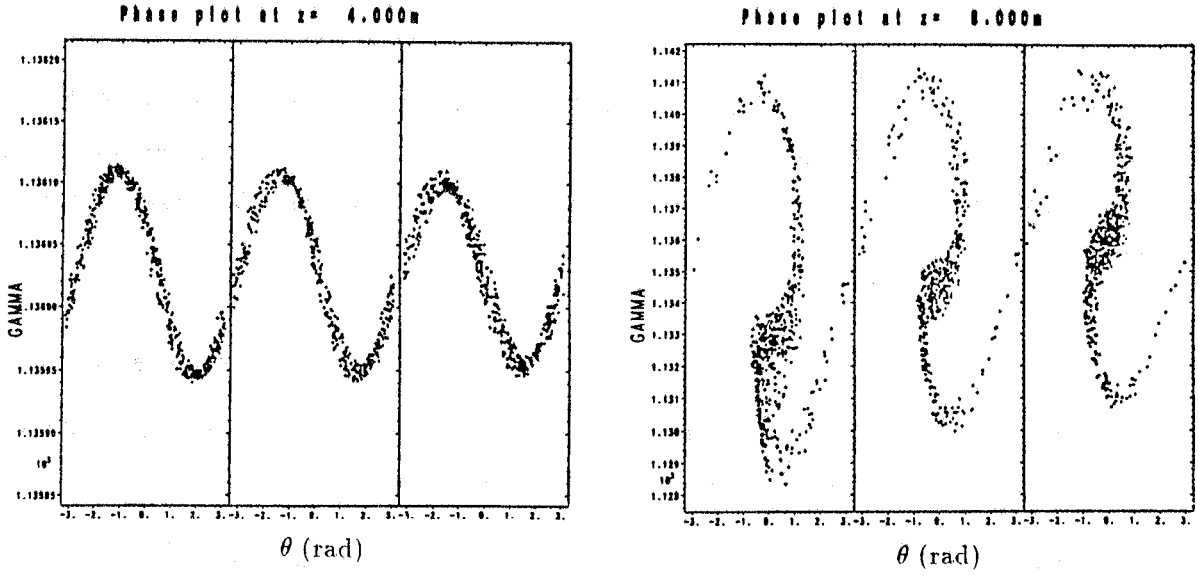

Figs. 14 a & b - Longitudinal phase spaces for the electron beam of the FRED-3D simulation at two different positions along the wiggler:

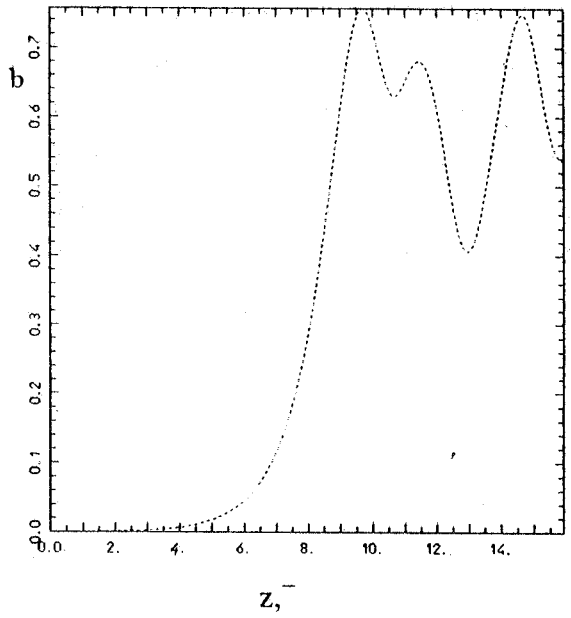

Fig. 15 - Beam bunching along the wiggler for the sets of parameters presented in Table 2, column 3.

The separation of the electron and the radiation beam can be achieved via a small magnetic deflection at the end of the first wiggler: such a deflection must of course ensure that the

debunching effect on the beam is negligible with respect to the radiation wavelength scale. Since to the first order, the path length difference, ΔL, for a beam with energy spread $\Delta\gamma/\gamma$ deflected by a magnet of angle θ (assumed small) and radius of curvature ρ_b is given by:

$$\Delta L \approx \rho_b \frac{\Delta\gamma\,\theta^3}{6\gamma}$$

setting $\rho_b = 2$ m (B = .96 T at 580 MeV) and $\theta = 5$ mrad, ΔL is less than 1 nm for $\Delta\gamma/\gamma$ of the order of 1 %, as typical near the saturation. Over 1 m, which could be the separation of the two wigglers (in order to achieve a shift of a few mm between the beam and the radiation) the path length difference due to the emittance, given by:

$$\Delta L \approx \frac{L\,\Delta\theta^2}{2}$$ where $\Delta\theta$ is the rms beam divergence

is of the order of 1 nm. Therefore the debunching effect at the entrance of the radiator can be kept small with respect to the radiation wavelength (20 nm).

Other possibilities to achieve the beam-field separation such as thin radiation absorbers or wiggler truncations (no half period at the wiggler end) must be investigated, but could in principle be exploited.

In order to evaluate the field power generated in the radiator we apply a cut to the numerical integration of the FEL-Compton equation[9], which corresponds to the first wiggler exit. At the cut (working actually as a variable threshold) we simply reduce the field intensity to zero, we keep the particle phase space unaltered (assuming zero debunching in the transport between the two wigglers) and we insert the new resonance condition (proper of the radiator) by zeroing the detuning. This is simply achieved by keeping $\langle p \rangle = 0$, i.e. by summing the quantity $\langle p \rangle$ at the threshold to all the particles, where $\langle p \rangle$ is the normalized detuning, given by:

$$\langle p \rangle = \frac{\langle \gamma - \gamma_r \rangle}{\rho \gamma_r}$$

That is equivalent to shift the resonant wavelength to the new value - proper of the radiator - which is determined by the beam energy at the end of the first wiggler.

In the present case the beam energy loss in the first wiggler, $\delta\gamma$, is always small - .04% ÷.15% of its initial energy - hence the wavelength increase, $\delta\lambda_r$, of the radiation emitted in the radiator is very small with respect to the resonant wavelength, λ_r, of the first "bunching" wiggler, according to the equation:

$$\frac{\delta\lambda_r}{\lambda_r} = -2\frac{\delta\gamma}{\gamma} \leq .3\,\%$$

The field power generated in the radiator is plotted in Fig. 16 versus the cumulative length of the system buncher wiggler - radiator, for three different threshold positions. The crosses show the standard steady state behaviour of the field power (i.e. for a buncher wiggler extending without any threshold) with a saturation level of 550 MW at z = 10.5 m: the curve is plotted just for reference. The solid line, the dashed line and the dotted one mark the field growth in the radiator when the length of the buncher wiggler is 8 m, 8.8 m and 9.6 m respectively. When the threshold is located at z = 8.8 m one gets 100 MW of field power from the first wiggler, then with two meters of radiator length (from z = 8.8 m to z = 10.8 m) the coherent spontaneous emission grows to 700 MW and then saturates again. Shifting the threshold towards larger z's causes the radiation to saturate in a shorter length (from z = 9.6 m to z = 10.9 m) lowering at the same time the power level (260 MW).

Since the threshold variation requires a variable length of the buncher wiggler (which can cause serious technological problems), the same effect can be achieved by varying the input signal power and taking a fixed buncher wiggler length, as shown in Fig. 17. Here the buncher wiggler length is assumed to be 8 m and the radiator starts at z = 8 m. The effect on the longitudinal phase of the beam transport from the wiggler to the radiator is neglected. As in Fig. 16, the crossed line shows the standard steady state exponential growth, while the other lines show the field power in the radiator for three different input powers at the entrance of the buncher wiggler: the solid line is referred to 100 W, the dashed to 400 W and the dotted one to 1000 W.

In Fig. 18 the bunching factor, b, is plotted for the same cases versus the cumulative length of the buncher wiggler-radiator system. It is clearly visible that the dashed line, corresponding to the 400 W input signal case which has the maximum field power generated in the radiator, has also the higher bunching level, fairly constant between z = 8 m and z = 10 m, where the saturation is reached in the radiator.
Moreover the solid line clearly exhibits a departure from the exponential law, also typical of the bunching in the steady state high gain regime: the field power is not growing exponentially in the radiator, as shown in Fig. 19, where the logarithm of the field power is plotted for the steady state and for the three different threshold positions.

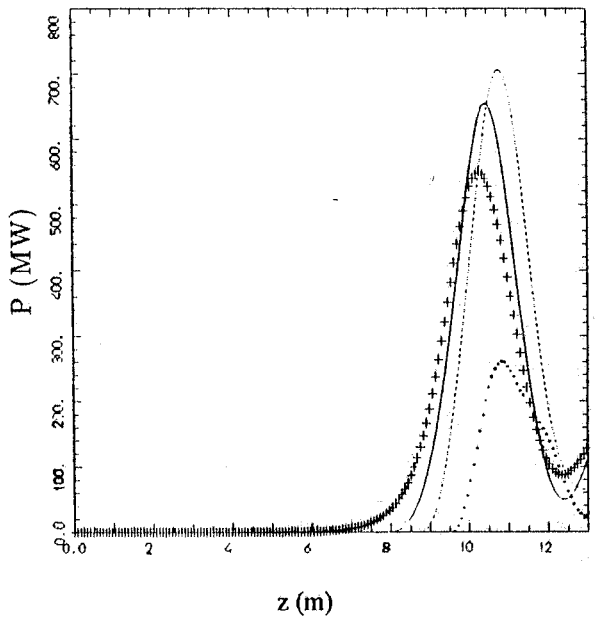

Fig. 16 - Field power generated in the radiator versus the cumulative length of the system buncher wiggler - radiator for three different threshold positions: the crossed line shows the standard steady state behaviour, whereas the solid line, the dashed line and the dotted one mark the field growth in the radiator when the length of the buncher wiggler is 8 m, 8.8 m and 9.6 m respectively.

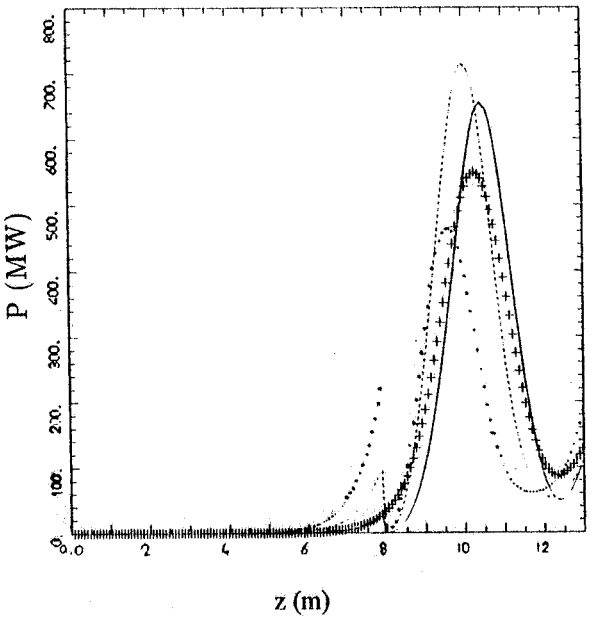

Fig. 17 - As Fig. 16, but varying the input signal power at the buncher wiggler entrance and taking a fixed buncher wiggler length (z = 8 m). The crosses show the standard steady state exponential growth (no threshold on the buncher wiggler, 100 W of input power), while the other lines show the field power in the radiator for three different input power signals: the solid line refers to 100 W, the dashed to 400 W and the dotted one to 1000 W.

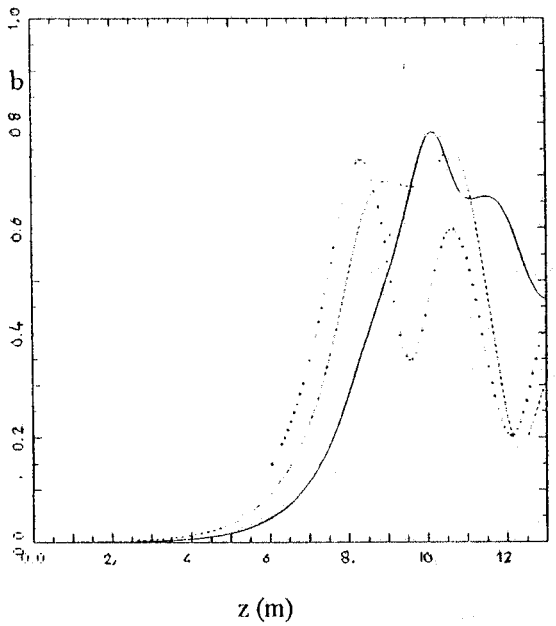

Fig. 18 - The bunching amplitude, b, plotted for the same cases of Fig. 17 versus the cumulative length of the buncher wiggler-radiator system.

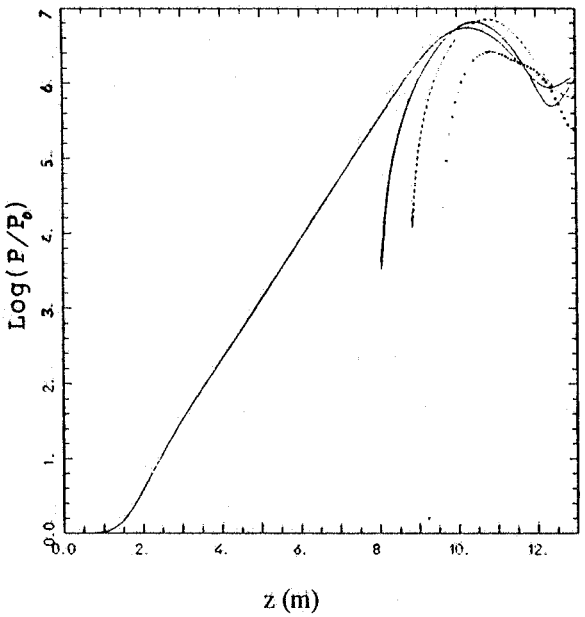

Fig. 19 - The logarithm of the field power in the radiator plotted for the steady state and for the three different threshold positions, specified in Fig. 16.

We can interpret the emission in the radiator in the following way: the bunched beam, once injected into the radiator is initially superradiant since it does no longer interact with the radiation field that caused the bunching. The coherent radiation generated has an intensity (before saturation) scaling with $b^2 \cdot N^2$ (N is the electron number) and grows very rapidly, as shown in Fig. 20, where a peak gain of 60-70 dB/m is reached in the first part of the radiator. This value is one order of magnitude higher with respect to the 8 dB/m of the steady state exponential gain.

It is interesting to notice that the radiated field still reaches saturation. This is due again to the potential well produced by the radiation, in which the electrons are trapped: when the electron oscillation period in the potential well is fairly equal to the exponential growth rate the electron beam starts to absorb energy from the radiated field. The OK experiments at Orsay are very similar to this scheme, with the exception that they operate in the low gain domain, where saturation cannot be reached, and the bunching can be assumed constant[16].

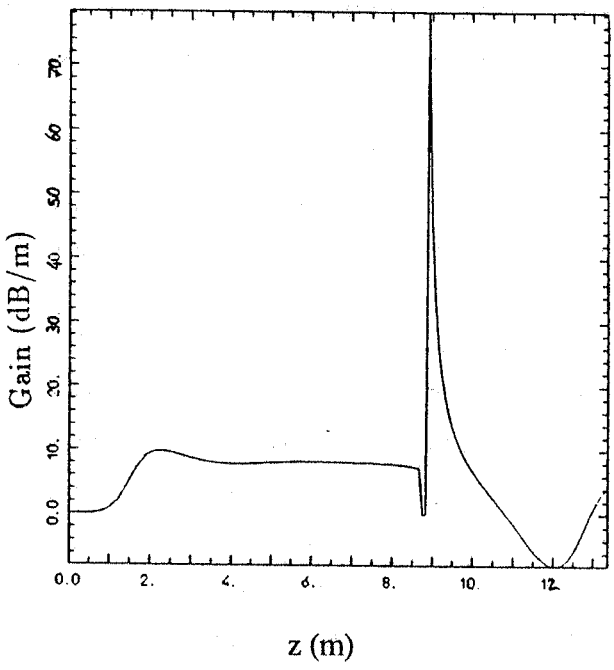

Fig. 20 - Coherent radiation growing in the wiggler-radiator system. A peak gain of 60-70 dB/m is reached in the first part of the radiator. This value is one order of magnitude higher with respect to the 8 dB/m of the steady state exponential gain.

In some sense the first part of the radiator shows a transient superradiant behaviour, involving all the electrons in the bunch: the observed superradiance is only transient since the slippage effects are, in our case, negligible, hence the field is always "sitting" on the electrons of the beam, interacting with them. The transient superradiance is therefore switched off when

the field intensity grows and the bunching is no longer constant. To evaluate the coherence quality of the radiated field we can assume a constant bunching and use the formula[15]:

$$\frac{dP_{coh}/d\Omega}{dP_{inc}/d\Omega} \approx |b|^2 \zeta$$

which gives the ratio between the coherent power radiated per unit solid angle and the incoherent one. ζ is the number of electrons in the coherence length $N_w \lambda_r$ of the radiation, N_w being the number of the radiator periods.

Assuming in our case: $|b|^2 \approx .35$, $N_w = 100$ and $\zeta \approx 10^7$, the ratio between the coherent power and the incoherent one is in the order of 10^6.

5 - HASW: Harmonic Switching and Far Future Experiments

In the first wiggler, the buncher wiggler, the beam is bunched not only on the fundamental but also on higher harmonics. It is well known that in a planar wiggler only the odd harmonics are present on axis. The dimensionless field intensity $|A|^2$ and the bunching on the fundamental harmonic are plotted in Fig. 21 as a function of the dimensionless wiggler length $z,^{-} = 4\pi\rho z/\lambda_w$ for a typical case with $a_w = 1.48$, while the bunching on the higher harmonics is plotted in Fig. 22. The third and fifth harmonic bunchings are quite pronounced (.3 and .5 respectively) just before saturation: that clearly indicates the possibility to use a radiator tuned not on the fundamental but on a higher harmonic.

This idea has already been exploited by the OK experiments in Orsay[16,17,18] and has recently been proposed in the high gain domain with a varied scheme[19]. Nevertheless, the novelty of our wiggler+radiator scheme is that we do not take the radiation from the first wiggler into the radiator, but we transfer only the bunched beam. The rational for this, in this range of wavelengths, is to avoid any phase slips between the beam and the radiation field generated in the passage from the buncher wiggler to the radiator wiggler. In fact, at the entrance of the radiator, a change in the relative phase can cause a shift in the beam-field coupling from an emission regime to an absorption one. It must be stressed that a difference of only 1 nm between the path lengths of the electron beam and of the radiation field produces, with a radiation wavelength of 5 nm, a significant change in the relative phase. In this case the electron beam, at the radiator entrance, is no longer in-phase with the radiation field, fact that causes a dramatic decrease of the radiation field and, eventually, of the beam bunching all along the first part of the radiator wiggler. In this respect, the relevance to cut out the beam-field interaction, avoiding to inject the radiation field into the radiator, is straightforward.

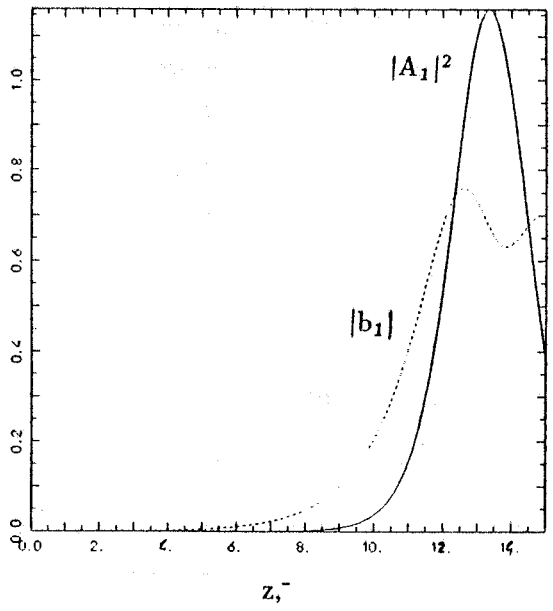

Fig. 21 - Dimensionless field intensity and bunching on the fundamental first harmonic along a wiggler with $a_w = 1.48$ (see text for details)

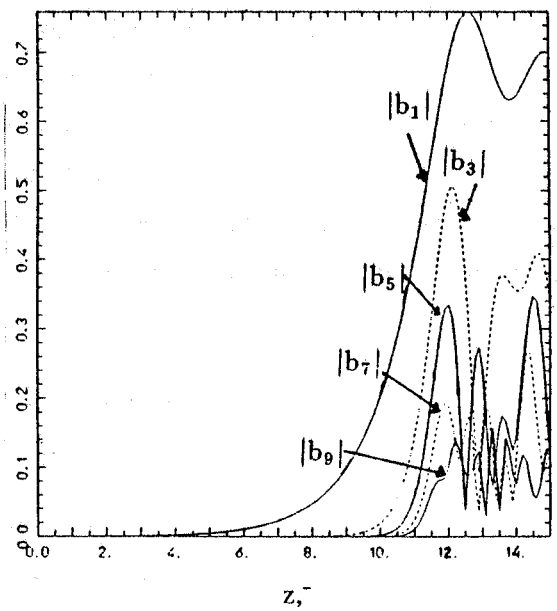

Fig. 22 - Higher harmonic bunching parameters for the same wiggler as in Fig. 21

Since the previously illustrated possible experiments are foreseen with a radiation wavelength in the range of 20÷50 nm, it is a natural choice to consider a jump in frequency of a factor 5 in order to point directly towards ≈ 5 nm, i.e. towards the so called "water window". The experiment described in the following will therefore deal with a fifth harmonic switching, but the scheme is in principle completely general and applicable to other harmonics.

The main parameters of the foreseen experiment are listed in Table 3. Recirculating the beam twice in the L3 section of the ARES Linac, its energy can be boosted to 820 MeV: in the first wiggler the beam radiates at a fundamental wavelength of 25 nm plus the higher odd harmonics.

Adding a slight ion focussing, one can achieve $\rho = 2 \cdot 10^{-3}$ and reach, after a 14 m wiggler, a fifth harmonic bunching, b_5, of the order of 0.05. The added ion focussing must be kept low in order to avoid too short Rayleigh lengths: at this wavelength the beam is very fine and the diffraction effects can dominate. In our case we choose a safe value for the parameter f_3, i.e. $f_3 = .82$.

Injecting now the beam into the radiator, whose fundamental is tuned at 5 nm (the fifth harmonic of the previous wiggler), we achieve coherent emission at 5 nm with a quasi-exponential growth of the radiation.

The dimensionless field intensity and the bunching on the fundamental in the buncher wiggler, i.e. $\lambda_r = 25$ nm, are plotted in Fig. 23 up to the dimensionless $z,¯ = 10.5$: thereafter the bunching and the dimensionless field intensity are referred to the fundamental of the radiator wiggler, i.e. $\lambda_r = 5$ nm, plotted up to $z,¯ = 20$.

The corresponding field power is shown by the dashed line plotted in Fig. 24, where 50 MW at $\lambda_r = 25$ nm are generated in the buncher wiggler (14 m long). The saturated power level in the radiator wiggler (10 m long, from z = 14 m to z = 24 m) is 160 MW at $\lambda_r = 5$ nm. The logarithm of the field power, plotted in Fig. 25, clearly shows that the field growth in the radiator has an initial very rapid but non-exponential behaviour, followed by a quasi-exponential one (i.e. quasi linear on a log. scale) up to the saturation.

Table 3 - HASW Experiment Main Parameters

	T [MeV]	I [A]	ε_n [m rad]	$\Delta\gamma/\gamma$ [keV]
Beam Parameters	820	400	$3 \cdot 10^{-6}$	± 250

	λ_w[cm]	λ_r[nm]	B_w[T]	H	R_b[μm]	ρ	f_3	f_1
Buncher wiggler	4	25	.56	.5	92	$2 \cdot 10^{-3}$	.82	
5th Harm. Radiator	2	5	.41	.1	50	$1 \cdot 10^{-3}$		2.35

	P_{sat}[MW]	I_{sat}[W/cm^2]	Photon Num.	q_f
Radiation parameters for λ_r = 5 nm	140	$1.8 \cdot 10^{12}$	$6.5 \cdot 10^{12}$	$4 \cdot 10^{-5}$

The bunching on the fundamental harmonic of the radiator (i.e. on the fifth harmonic of the buncher wiggler) is indeed low at the radiator entrance, around 0.05, hence the radiation emission is no longer a pure coherent spontaneous emission as in the case of the previous section, where the bunching was 0.5. In this case the bunching and the field grow together in a way more similar to the standard steady state regime. Cutting the buncher wiggler at z = 13 m the fifth harmonic bunching is now lower: $|b_5| = .001$. The evolution of the field power and of the bunching in the radiator, shown by the solid line of Fig. 25 and 26 respectively, are more similar to the exponential gain regime, with a saturated power level at 320 MW. This larger value is due to the lower energy spread achieved by the beam at the end of the buncher wiggler.

Such a spread, which is modulated on the scale of the fundamental radiation wavelength $\lambda_r = 25$ nm, grows in the buncher wiggler together with the bunching b_1. At the entrance of the radiator the spread on $\lambda_r = 25$ nm acts as an incoherent beam spread since the radiator is tuned at the lower wavelength $\lambda_r = 5$ nm.

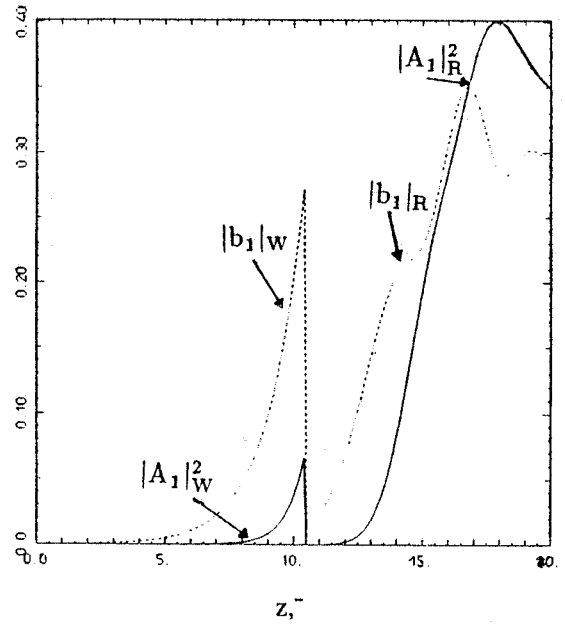

Fig. 23 - Dimensionless field intensity (solid line) and bunching (dashed line) for the $\lambda_r = 25$ nm ($z,^{\sim} < 10.5$) in the buncher wiggler and for $\lambda_r = 5$ nm ($z,^{\sim} > 10.5$) in the radiator. (see text for details).

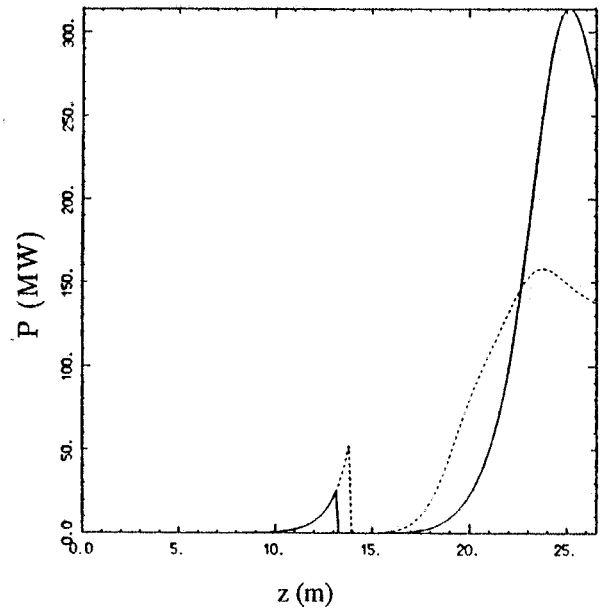

Fig. 24 - Field power growth at $\lambda_r = 5$ nm for two different lengths of the buncher wiggler (see text for details).

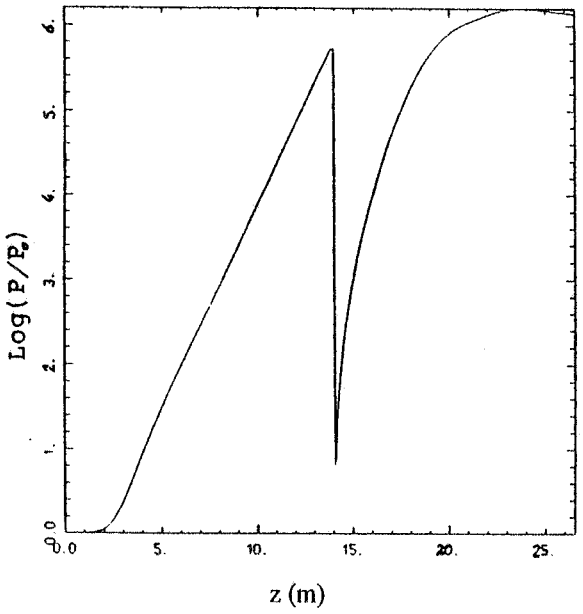

Fig. 25 - Logarithm of the field power on $\lambda_r = 25$ nm (for $z<14$ m) in the buncher wiggler and on $\lambda_r = 5$ nm (for $z>14$ m) in the radiator (see text for details).

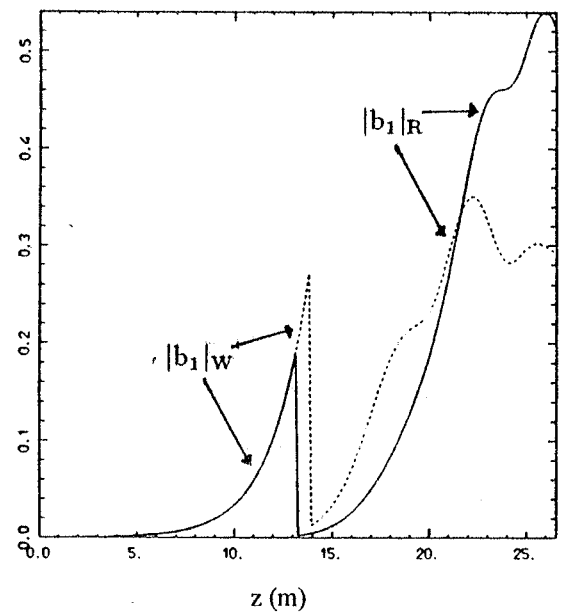

Fig. 26 - Bunching parameter amplitude in the buncher wiggler and in the radiator for two different buncher wiggler length (see text for details).

We can conclude that higher is the value of $|b_5|$ at the radiator entrance, more is the incoherent energy spread of the beam and lower is the gain in the radiator. Since the emittance condition relationship (2) is violated inside the radiator ($f_1 = 2.35$), one would like to have the highest possible $|b_5|$ at the radiator entrance in order to overcome the emittance condition, which is strictly true for an unbunched beam. Hence a trade off between the two opposite requirements must be found: 3-D simulations are needed to evaluate what is the maximum value of f_1 (as a function of the bunching $|b_5|$ at the entrance) which ensures an acceptable gain deterioration.

The electron longitudinal phase spaces along the radiator are shown in Fig. 27a to 27d . The phase space, extending in the buncher wiggler over 2π radians of the radiation $\lambda_r = 25$ nm, is scaled at the radiator entrance over the corresponding 10π radians of the $\lambda_r = 5$ nm. The energy spread on the scale of the wavelength $\lambda_r = 25$ nm is clearly visible (the spread is normalized to the parameter $\rho = 1 \cdot 10^{-3}$). Since the radiation at 25 nm is no more resonant in the radiator, the onset of the radiation at 5 nm stimulates the bunching over the five buckets contained between 0 and 10π of the phase space. At z = 18 m, slightly before saturation, the bunching on the radiation at 5 nm is clearly visible. The initial energy spread has been taken as the expected spread of the beam, $\Delta\gamma/\gamma = \pm 3 \cdot 10^{-4}$

The coherence of the radiated field can be estimated assuming a constant $b_5 \approx 0.1$: the ratio between coherent and incoherent power per unit solid angle comes out to be $1.7 \cdot 10^{-5}$, which is just consistent with the quantum fluctuation parameter, $q_f \approx 4 \cdot 10^{-5}$.

6 - Conclusion

The high energy particle accelerator community agrees that one of the most relevant topic, on the way of the TeV electron-positron collider realization, is the capability to generate electron beams with high peak current and very low normalized emittance. The construction of an intermediate energy LINAC able to produce high quality beams seems to be a necessary step towards the TeV collider. In this respect, a soft X-ray FEL must be viewed as a test bench of the beam quality achieved. We have shown that with the ARES SC Linac facility several experiments in this context are envisageable: the link X-ray FEL's - SC LINAC's will hopefully be a marriage of convenience.

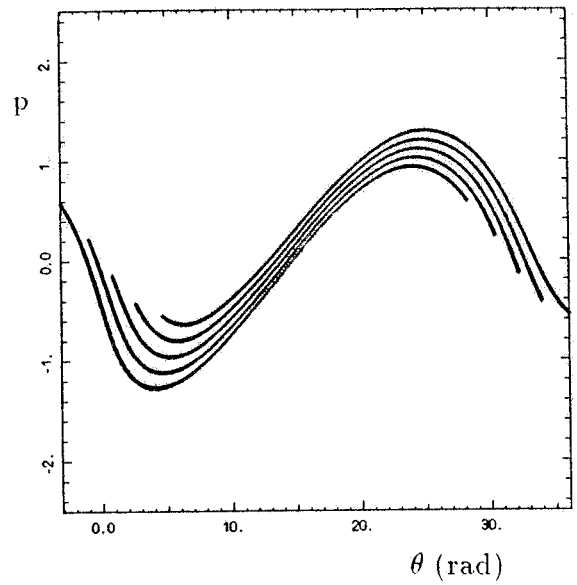

Fig. 27a - Longitudinal phase space at the buncher wiggler exit (z = 14 m).

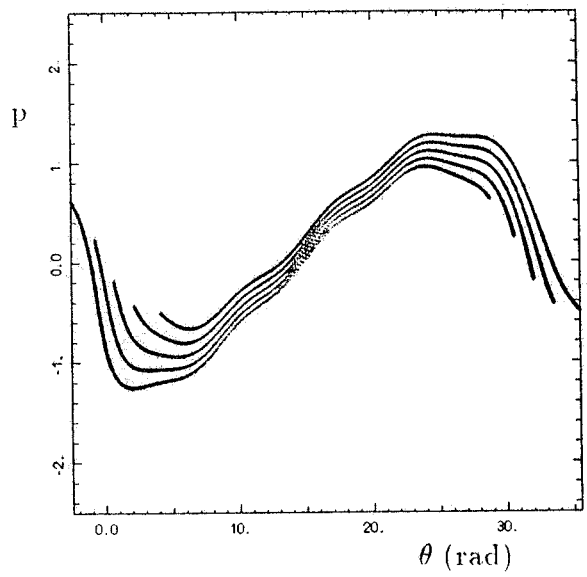

Fig. 27b - Longitudinal phase space at z = 15.3 m (1.3 m far from the radiator entrance)

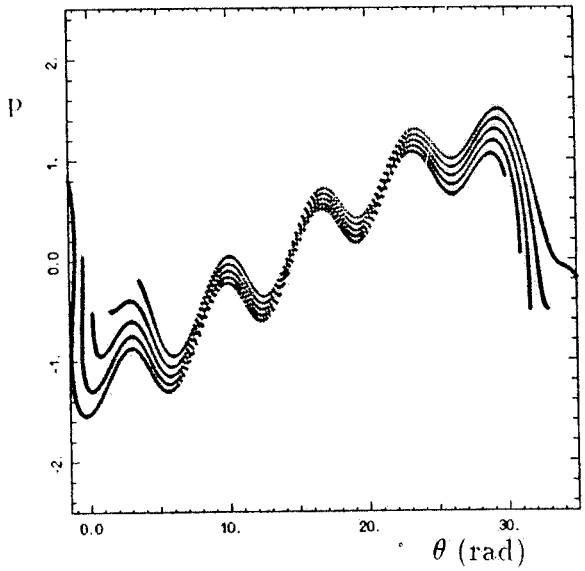

Fig. 27c - Longitudinal phase space at z = 16.7 m (2.7 m far from the radiator entrance)

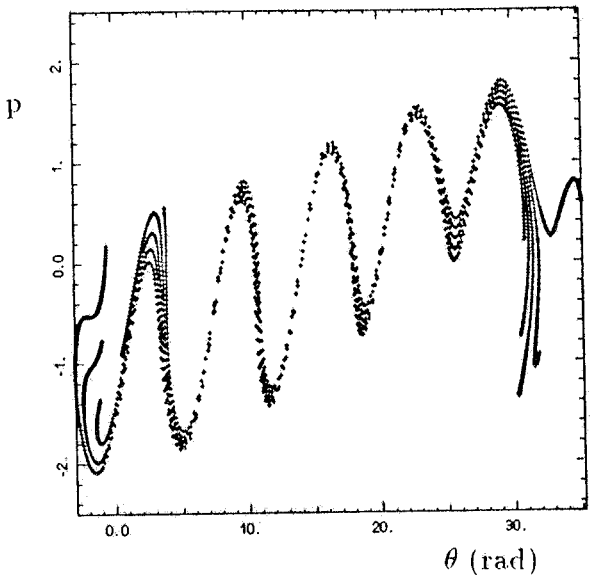

Fig. 27d - Longitudinal phase space at z = 18.8 m (4 m far from the radiator entrance)

Acknowledgments

We are indebted to W.A.Barletta and A.M.Sessler for their support and encouragement in proposing the X-VUV FEL experiments in the ARES project context. We thank especially W.A.Barletta for the numerical simulations made with FRED-3D and we are also grateful to G.Vignola and M.Castellano for helpful and valuable discussions.